

1 **Title:** SARS-CoV-2 evolution in the absence of selective immune pressures, results in antibody
2 resistance, interferon suppression and phenotypic differences by lineage.

3 **Authors:** Julian Daniel Sunday Willett^{1,2,3}, Annie Gravel⁴, Isabelle Dubuc⁴, Leslie Gudimard⁴,
4 Ana Claudia dos Santos Pereira Andrade⁴, Émile Lacasse⁴, Paul Fortin^{4,5,6}, Ju-Ling Liu^{2,8}, Jose
5 Avila Cervantes^{2,8}, Jose Hector Galvez⁷, Haig Hugo Vrej Djambazian^{2,8}, Melissa Zwaig^{2,8}, Anne-
6 Marie Roy^{2,8}, Sally Lee^{2,8}, Shu-Huang Chen^{2,8}, Jiannis Ragoussis^{2,8*}, Louis Flamand^{4,9*}

7

8 **Affiliations:**

- 9 1. Quantitative Life Sciences Ph.D. Program, McGill University, Montreal, QC, Canada
10 2. McGill Genome Centre, McGill University, Montreal, QC, Canada
11 3. Lady Davis Institute, Jewish General Hospital, Montreal, QC, Canada
12 4. Axe maladies infectieuses et immunitaires, Centre de Recherche du Centre Hospitalier
13 Universitaire de Québec- Université Laval, Canada
14 5. Centre de Recherche ARThrite-Arthrite, Recherche et Traitements, Université Laval,
15 Québec, QC, Canada
16 6. Division of Rheumatology, Department of Medicine, CHU de Québec-Université Laval,
17 Québec, QC, Canada
18 7. Canadian Centre for Computational Genomics, McGill University, Montreal, QC, Canada
19 8. Department of Human Genetics, McGill University, Montreal, QC, Canada
20 9. Département de microbiologie-infectiologie et d'immunologie, Université Laval, QC,
21 Canada

22 *Co-corresponding authors

23

24 **Abstract:**

25 The persistence of COVID-19 is partly due to viral evolution reducing vaccine and treatment
26 efficacy. Serial infections of Wuhan-like SARS-CoV-2 in Balb/c mice yielded mouse-adapted
27 strains with greater infectivity and mortality. We investigated if passaging unmodified B.1.351
28 (Beta) and B.1.617.2 (Delta) 20 times in K18-ACE2 mice, expressing human ACE2 receptor, in
29 a BSL-3 laboratory without selective pressures, would drive human health-relevant evolution
30 and if evolution was lineage-dependent. Late-passage virus caused more severe disease, at
31 organism and lung tissue scales, with late-passage Delta demonstrating antibody resistance
32 and interferon suppression. This resistance co-occurred with a *de novo* spike S371F mutation,
33 linked with both traits. S371F, an Omicron-characteristic mutation, was co-inherited at times
34 with spike E1182G per Nanopore sequencing, existing in different quasi-species at others. Both
35 are linked to mammalian GOLGA7 and ZDHHC5 interactions, which mediate viral-cell entry and
36 antiviral response. This study demonstrates SARS-CoV-2's tendency to evolve with phenotypic
37 consequences, its evolution varying by lineage, and suggests non-dominant quasi-species
38 contribute.

39 **Keywords: SARS-CoV-2, COVID-19, pandemic modelling, treatment resistance, viral**
40 **evolution.**

41 **Introduction:**

42 Part of the difficulty in responding to the COVID-19 pandemic has been predicting viral evolution
43 and its impact on clinically relevant traits, such as disease severity, infectivity, and treatment
44 resistance¹. The basic biology of the severe acute respiratory syndrome Coronavirus 2 (SARS-
45 CoV-2), the virus that causes COVID-19, is well understood². However, knowledge of SARS-
46 CoV-2 evolution is limited. Many RNA viruses, like SARS-CoV-2, exist as quasi-species
47 meaning that within a given viral population, a multitude of alleles (major and minor) are
48 present. These alleles give plasticity to the viral population allowing for rapid
49 adaptation/selection to a variety of circumstances³. Viral evolution is also complex and affected
50 by several factors, including host genetic background⁴, host immune status⁵, the organs
51 targeted by the virus⁶, and a population's collective immunity⁷. As a result, it has been difficult to
52 predict the emergence of new variants with altered virulence.

53 Several SARS-CoV-2 variants of concern (VOC) have emerged, each with mutations providing
54 dissemination advantages¹. The SARS-CoV-2 Alpha variant (B.1.1.7) gained a growth
55 advantage and rapidly spread globally due to the spike protein N501Y mutation that enhanced
56 affinity for the cellular entry receptor, angiotensin-converting enzyme 2 (ACE2)⁸. Other VOC,
57 such as the Delta (B.1.617.2) variant, gained advantages with additional spike substitutions,
58 including L452R⁹, T478K¹⁰, and P681R¹¹ that affect viral transmissibility and antibody
59 neutralization for naturally or artificially vaccinated individuals¹². To better predict changes in
60 SARS-CoV-2 and reduce the impact of a future pandemic, time-effective models must be
61 defined for studying viral changes over successive generations and characterizing their
62 evolutionary consequences.

63 In 2020, Gu *et al.* studied short-term viral evolution by infecting aged mice with the SARS-CoV-2
64 reference strain (IME-BJ05) and collecting lung tissue at set timepoints following infection, using

65 this isolate to infect successive generations of mice¹³. While wild-type mice are considered to be
66 less susceptible to the virus since mouse Ace2 is not used by SARS-CoV-2 as its receptor, Gu
67 *et al.* demonstrated that serial passaging of infected lung homogenate across mice produced a
68 mouse-adapted strain (MASCp6) that causes pulmonary symptoms, matching adaptations
69 observed by others who previously applied the technique to influenza^{13,14}. After six passages,
70 they found several clinically relevant genetic changes, including the *de novo* appearance of
71 A23063T that causes the spike mutation N501Y¹³. This mutation is associated with enhanced
72 viral infection and transmission⁸. Subsequently, the group passaged the MASCp6 isolate an
73 additional 30 times and characterized the MASCp36 isolate¹⁵. MASCp36 contained several
74 mutations (K417N, Q493H, N501Y) in the spike protein conferring greater mouse Ace2 receptor
75 binding affinity, increased infectivity and greater virulence¹⁵. Others replicated this study using
76 the same viral variant, observing similar development of clinically relevant variant alleles¹⁶.

77 Since these studies, new VOC have arisen with the latest being Omicron, negatively impacting
78 treatment efficacy¹. Others have studied viral dynamics using recent lineages in serial passages
79 in cells, observing similar development of directional selection and clinically concerning
80 mutations with contributions by quasi-species^{17,18}. Understanding longitudinal viral changes in a
81 mammalian host is pressing. We adapted Gu *et al.*'s approach¹³ to determine if more recent and
82 human-adapted lineages, B.1.351 (Beta) and B.1.617.2 (Delta), evolved over a twenty passage
83 study in transgenic mice expressing the human ACE2 receptor, if this evolution varied by
84 lineage, and whether these changes were relevant to human health. We used transgenic
85 animals to limit selective pressure and adaptations to the murine ACE2 receptor, as occurred in
86 Gu *et al.*'s works^{13,15}. We report on virus evolving in the setting of no experimental selective
87 pressures with changes observed at the organism, tissue, and genetic scale, this evolution
88 varying by lineage with solely late-study Delta lineage presenting characteristics resulting in

89 decreased antibody neutralization, with variant alleles arising *de novo* that have been linked
90 with these phenotypes.

91

92 **Results:**

93 *Late passaged virus produced more viral RNA, greater weight loss, and worse lung*

94 *inflammation. Only late-study Delta was associated with increased viral load and cytokine*

95 *changes linked to severe COVID-19.* To study evolution on the organism level, we compared

96 clinical scores of mice infected with early and late passaged virus (**Figure 1**). Unlike Gu *et al.*'s

97 study that required adaptation of SARS-CoV-2 to a murine Ace2 receptor for infectivity, our

98 study used transgenic mice expressing the human ACE2 receptor¹³. On day 3 post-infection,

99 lungs of passage [P]20 Beta and Delta infected mice contained significantly more SARS-CoV-2

100 RNA than corresponding P0 viruses (**Figure 2A**). Mice infected with P20 Delta virus had a

101 significant increase (6.3x) in lung viral loads relative to P0 (**Figure 2B**) ($p=0.008$) with no

102 difference for Beta P0 and P20 (**Figure 2B**). Both P20 Beta and Delta viruses caused more

103 rapid and greater weight loss than P0 (**Figures 2C-D**) with similar survival curves (data not

104 shown).

105 To determine if the significant increase in lung viral load observed by Delta virus was related to

106 growth kinetic differences between P0 and P20 viruses, we performed *in vitro* growth curve

107 analysis. Using two independently evolved P20 Delta viruses, we observed that P20 viruses

108 yielded significantly (4-5X) more infectious virus after 24h of infection versus Delta P0 virus ($p =$

109 0.02) (**Figure 3**). This difference in viral titers was no longer observed after 48 h of infection

110 (**Figure 3**).

111 Lungs of mice infected with P0 and P20 viruses were examined for signs of inflammation as

112 assessed by histology and presence of inflammatory cytokines. On day 6 post-infection, P20

113 Beta and Delta viruses caused greater leukocyte infiltration, red blood cell extravasation, and
114 decreased alveolar space versus P0 and mock-infected mice (**Figures 4A-E**). Lung tissues
115 were also analyzed for SARS-CoV-2 antigenic burden and leukocyte recruitment as measured
116 using anti-N and anti-CD45 antibodies, respectively. Results indicated that significantly more
117 cells were expressing N by Beta P20 than P0, with no change by passage for Delta (**Figure 5**).
118 While Delta had significantly greater immune cell infiltration than Beta per CD45 staining,
119 immune infiltration did not significantly change between P0 and P20 for either lineage (**Figure**
120 **5**). On day 3 post infection, Beta P20 virus induced greater production of proinflammatory
121 CXCL1, CCL2 and IL-6 versus P0 (**Figures 6A-C**)¹⁹. Delta P20 infection resulted in diminished
122 IFN- β and IFN- γ production versus P0, which correlated with the increased viral load and has
123 been linked with more severe COVID-19 in humans^{20,21} (**Figures 6D-E**).

124 We next assessed whether repeated passages in K18-ACE2 mice would select for viruses
125 capable of infecting non transgenic mice. C57BL6 (B6) mice were infected intranasally with P0
126 and P20 Beta and Delta viruses and lung SARS-CoV-2 RNA and infectious viral loads
127 determined 3 days later. Both P0 and P20 Beta viruses successfully replicated in B6 mouse
128 lungs with both viruses producing similar SARS-CoV-2 RNA and infectious viral loads
129 (**Supplementary Figure 1**). None of the P0 or the P20 Delta virus infected mice had detectable
130 SARS-CoV-2 RNA or infectious viral loads above the limit of detection (**Supplementary Figure**
131 **1**).

132
133 *Late-study Delta, not Beta, virus presented with greater antibody resistance.* We next
134 determined the ability of sera from vaccinated subjects to neutralize passaged viruses,
135 comparing it to stock P0 viruses. Consistent with previous reports, sera from vaccinated
136 subjects had varying neutralizing potential depending on the variant, with neutralization titers
137 being greatest against the original Wuhan-like strain and lowest for the Beta isolate (**Figure**

138 **7A**)^{22,23}. The same sera were analyzed for their ability to neutralize P20 viruses. P20 Beta was
139 neutralized equally (13 out of 24) or more efficiently (8 of 24) than the P0 virus (**Figure 7B**). In
140 contrast, P20 Delta virus was significantly less sensitive to antibody neutralization by vaccinated
141 subject sera than P0 ($p < 0.0002$) with 15 of 24 sera showing decreased neutralizing potential
142 toward the P20 Delta virus relative to P0 (**Figure 7C**).

143
144 *Variant alleles associated with COVID-19 severity and susceptibility, cytokine suppression, and*
145 *antibody resistance arose de novo predominantly in late passaged Delta virus.* To link
146 phenotypic changes with genetics, we identified those variant alleles that changed in frequency
147 across passages, including those that arose *de novo* and disappeared, and annotated them for
148 traits with implications on public health, such as conferring antibody resistance. Variant allele
149 frequency across passages and between samples in single passages did not statistically
150 change (adjusted p -value ≥ 0.05), except when comparing Beta P17 and P20 to earlier
151 passages and Delta P10 and P20 (**Supplemental Figure 2a-b**). Given no significant change in
152 mean allele depth, these differences could be due to growing allelic diversity and within-host
153 evolution of quasi-species, per Tonkin-Hill *et al.*²⁴. Sample contamination was less likely as
154 there was no significant difference in VAF or variant allele depth between samples for either
155 viral lineage (**Supplemental Figure 2c-d**).

156 Of 82 unique variant alleles, there were 26 that were nonsynonymous and appeared *de novo* or
157 whose allele frequency (VAF) clearly changed with 20 having immediately clinically-relevant
158 annotations, with 20 occurring in viral proteins that interact with human proteins, 1 believed to
159 confer drug resistance, 1 associated with the Omicron lineage, 1 linked with antibody escape,
160 and 7 at vaccine targets (**Table 1, Supplemental Table 1**)^{25,26}. These included 9 that were
161 specific to Beta, 16 that were specific to Delta, and 1 that changed in both lineages. The variant
162 allele associated with Omicron was C22674T (Spike S371F) that arose *de novo* in 2/3 animals

163 in P20 for Beta virus and 2/3 animals in P13 for Delta virus, persisting in later passages (**Figure**
164 **8, Supplemental Table 1**). We thus observed an Omicron specific mutation in a study not
165 involving Omicron viral lineages. The S371F mutation alters spike glycoprotein that interacts
166 with human proteins GOLGA7 and ZDHHC5, which contribute to viral-cell entry²⁷ and
167 palmitoylation that mediates viral infectivity²⁸, over-response to pathogens, and interferon
168 production²⁹. It has also been reported to undermine antibody response.³⁰

169 Of the variant alleles that changed in frequency, many involved viral proteins that interact with
170 human proteins suggested to influence COVID-19 severity and susceptibility, representing
171 druggable targets, and could explain phenotypes observed in this study (**Supplemental Table**
172 **1**). A929G (I222V), which arose and persisted in 1/3 animals infected with Delta in P17
173 (**Supplemental Figure 3**), involves nsp2 via ORF1ab that interacts with GIGYF2³¹. C10341T
174 and C10809T occur in nsp5 via ORF1ab (P3359L and P3515L), that interacts with HDAC2 that
175 has been identified to enable immune evasion as an anti-immune effector³². C10341T arose in
176 1/3 animals in P13 for Delta and likely persisted for remaining passages, with its absence in P17
177 perhaps due to sequencing error (**Supplemental Figure 3**). C10809T disappeared after P0 in
178 Beta, reappearing in 1/3 animals in P17 (**Supplemental Figure 3**). HDAC2 has four approved
179 gene family-specific inhibitors, such as vorinostat, and one approved activator, theophylline³³.

180 G28237T disappeared after P0, then reappeared in 3/3 animals infected with Beta by P20
181 (**Figure 8**). It occurred in ORF8 (R115L), which interacts with LOX, linked to COVID-19 severity
182 and thrombosis³⁴, PLOD2, linked to COVID-19 and respiratory failure³⁵, and FKBP10, linked to
183 poor COVID-19 prognoses³⁶. *LOX* can be targeted by 3 approved medications, including the
184 inducer cupric sulfate³³, *PLOD2* can be targeted by three approved medications, including a
185 cofactor ascorbic acid³³, and FKBP10 can be stimulated by bleomycin³⁷.

186 Most alleles in the P0 Beta isolate, passaged several times *in vitro* in Vero cells, encoded a
187 Spike protein with a tryptophan (W) at position 682 (C23606T), destroying the furin cleavage

188 site (**Table 1**). We observed a rapid selection of viruses having the reference allele encoding an
189 arginine (R) at position 682 and functional furin site in all animals infected with Beta variant
190 starting in P10 (**Table 1**). This suggests that the furin site provides a growth advantage under *in*
191 *vivo* conditions and supports a previous report indicating the Spike furin site being important for
192 SARS-CoV-2 virulence in K18-ACE2 mice³⁸.

193 Nanopore focused sequencing of the S (spike) gene suggested several of these variant alleles
194 were co-inherited by distinct Delta quasi-species. Spike mutations S371F and E1182G were
195 observed to occur at identical Nanopore-derived allele frequencies in P17 for animal two and
196 P20 for animal three, suggesting co-inheritance from P13 viruses. While only S371F and A892V
197 were observed to have the same allele frequency in P13 with E1182G not detected by
198 Nanopore in this passage, but detected by Illumina, this could be a product of sequencing error
199 or changes, alongside observing co-inheritance of alleles at distinct times in distinct samples
200 (**Figure 8**). S371F confers antibody escape with S371F and E1182G both interacting with
201 GOLGA7 and ZDHHC5, which enable viral cell entry²⁷ and infectivity²⁸.

202

203 **Discussion:**

204 In this work, we show that more recent and human-adapted lineages of SARS-CoV-2, Beta and
205 Delta, evolve in a setting of minimal selective pressures, Delta developed more clinically
206 relevant changes than Beta with both yielding more pronounced lung disease and disease
207 severity, and these phenotypic changes can be partially explained by discrete development and
208 disappearance of alleles linked with key traits, such as antibody resistance and interferon
209 suppression. Given our observance of these alleles with frequencies suggestive of minor quasi-
210 species, it could suggest their significance in COVID-19, experimentally supporting others'
211 conclusions in a controlled setting²⁴. While the evolution of the original SARS-CoV-2 strain in

212 Balb/c mice has been previously reported, with genetic changes used to explain phenotypic
213 evolution^{13,15}, Beta and Delta lineages are more genetically adapted to humans with additional
214 spike mutations, making a model more similar to humans with mice expressing human ACE2R
215 more pressing. This also limits selection for murine Ace2 adaptation, establishing a baseline for
216 a model to build off. Furthermore, none have compared the phenotypic changes of two lineages
217 in a single study, offering controlled, experimental evidence for lineage-based evolutionary
218 differences.

219 The Delta P0 virus, which lacked the N501Y mutation, never acquired it in our study. Acquisition
220 of N501Y in humans was reported almost a year after SARS-CoV-2 epidemic's beginning,
221 suggesting the mutation arose alongside growing herd immunity³⁹. This could suggest that in
222 the absence of selective immune pressure, such as neutralizing antibodies, or pressure to adapt
223 to murine ACE2, N501Y is not favored (**Figure 8**). Beta P0 harbored the N501Y mutation, which
224 was previously reported to enable reference SARS-CoV-2's adaptation in non transgenic
225 mice¹³. This mutation remained unchanged in our study, suggesting that our virus could infect
226 cells through the murine ACE2 receptor, which we demonstrated in non transgenic C57BL6
227 mice using Beta P0 and P20 viruses (**Supplementary Figure 1**). ACE2 transgene being more
228 widely expressed than murine ACE2 could explain the greater SARS-CoV-2 RNA loads in K18
229 mouse lungs versus B6. Beta's flexibility to use human and murine receptors could explain our
230 isolate's greater virulence versus others, such as Wuhan and Delta that lacked N501Y⁴⁰.

231 Evolved Beta and Delta modulated the inflammatory and antiviral responses differently than
232 corresponding P0 viruses, both causing greater and more rapid weight loss and more severe
233 lung damage without a significant change in detected inflammatory cells, suggesting mediation
234 by overactivation of existing cells or systemic factors (**Figure 5**). Beta P20 infection was
235 associated with greater inflammatory cytokine production (CCL2, CXCL1, IL-6) than P0 ($p <$
236 0.005 , $p = 0.051$, $p < 0.05$, respectively) (**Figure 6**). This occurred with the disappearance of

237 several variant alleles, and the *de novo* development of S371F in P20 for 2/3 animals (**Figure 8**,
238 **Supplemental Figure 3**). G23593T, or spike Q677H, which disappeared from Beta virus
239 samples after P0, enhances treatment resistance and increase viral infectivity⁴¹. The reversion
240 of Spike amino acid 677 to Q after passage in mice could explain the increased neutralization
241 activity for some of the sera against Beta P20 relative to P0 (**Figure 7**). Delta P20 infection
242 yielded greater viral load than P0 with suppressed IFN- β and IFN- γ , suggesting acquisition of
243 additional antiviral/immunomodulatory properties that could be mediated by S371F's (C22674T)
244 effect on spike protein, which can suppress type I interferon expression⁴². S371F, which arose
245 *de novo* and persisted in two animals in P20 for Beta and P13 for Delta virus (**Figure 8**), is one
246 of the 8 Omicron BA.2-specific spike mutations that induces a 27-fold reduction in the capacity
247 of sotrovimab to neutralize BA.2, broadly affecting the binding of most RBD-directed antibodies
248 (**Table 1**)³⁰. A929G (ORF1ab I222V) also arose *de novo* in 1/3 animals, which could impact
249 nsp2's suppression of GIGYF2's functions (**Table 1, Supplementary Figure 3**)³¹.

250 This study had limitations. We used K18-ACE2 transgenic mice but the mechanisms of new
251 viral variants arising in humans could significantly differ, which is relevant as host factors are
252 believed to contribute to viral variant allele diversity⁴³. Our model lacked experimental selective
253 pressures, while the COVID-19 pandemic has been accompanied by contact limitations and
254 vaccines with the dominant SARS-CoV-2 evolutionary mechanism believed to be natural
255 selection⁷. A baseline is required to effectively model these pressures. We studied Beta and
256 Delta lineage virus, which are no longer the dominant lineages and our conclusions could vary
257 with Omicron. This underscores the value in studying single-allele changes as they can capture
258 fitness-related traits.

259

260

261 **Conclusions:**

262 We demonstrate that more human-adapted SARS-CoV-2 lineages when passaged in mice
263 expressing human ACE2 receptor evolve in the setting of minimal selective pressures, their
264 changes vary by lineage, and accumulate clinically-relevant changes, such as antibody
265 resistance.

266

267 **Methods:**

268 **Viruses.** SARS-CoV-2 Wuhan-like strain (LSPQ, B1 lineage) was obtained from the Laboratoire
269 de Santé Publique du Québec ([LSPQ] Sainte-Anne-de-Bellevue, QC, Canada). SARS-CoV-2
270 Beta strain was obtained from BEI resources and SARS-CoV-2 Delta strain from the BC
271 Centers for Disease Control. Unmodified SARS-CoV-2 strains were propagated on Vero cells
272 (American Type Culture Collection, Manassas, Virginia, USA).

273 **Determination of the viral titer.** Vero cells were plated in a 96-well plate (2×10^4 /well) and
274 infected with 200 μ l of serial dilution of the viral preparation or lung homogenate in the M199
275 media supplemented with 10mM HEPES pH 7.2, 1mM of sodium pyruvate, 2.5g/L of glucose,
276 5 μ g/mL *Plasmocin*[®] and 2% FBS. Three days post-infection plates were analyzed using a
277 EVOS M5000 microscope (ThermoFisher Scientific, Waltham, MA, USA) and the viral titer was
278 determined using the Karber method ⁴⁴.

279 **Mouse models.** B6.Cg-Tg(K18-hACE2)2Prlmn/J (stock#3034860) and B6 mice were
280 purchased from the Jackson Laboratories (Bar Harbor, ME). All mouse studies were conducted
281 in a BSL-3 laboratory. One K18-ACE2 mouse was intranasally infected with either B.1.351
282 (Beta) or B.1.617.2 (Delta) SARS-CoV-2 lineages. Following 3-4 days, the animals were
283 sacrificed and lung homogenate collected. The homogenate was used to intranasally infect
284 sequential animals, defined as passage. This was repeated for 10 passages. After passage 10

285 (P10), virus in lung homogenate was sequenced. K18-ACE2 mice were then intranasally
286 infected with Beta P10 or Delta P10 with viruses passaged in three mice at a time for an
287 additional 10 times (total of 20 passages) with virus in lung homogenate sequenced following
288 passages 13, 17, and 20 (**Figure 1**). Viral stocks were then made from lung homogenates of
289 Beta and Delta P20 viruses. K18-ACE2 mice were infected intranasally with 500 TCID₅₀ of P0 or
290 P20 viruses. Lung viral loads were determined on day 3 post-infection with weight loss and
291 survival monitored daily for up to 9 days.

292 ***Infectivity of P0 and P20 viruses to non-transgenic mice.*** C57BL6 mice were infected
293 intranasally with 3000 TCID₅₀ of P0 and P20 Beta and Delta viruses. Three days later, mice
294 were euthanized, and lungs collected for viral load (titer) determination, as per previously
295 describe⁴⁵.

296 ***RNA extraction:*** Up to 30 mg of lung tissue were used for RNA extraction using the Bead Mill
297 Tissue RNA Purification Kit and the Bead Mill Homogenizer (Kennesaw, GA), following
298 manufacturer's instructions.

299 ***Droplet digital PCR (ddPCR) quantitation of SARS CoV-2 RNA.*** SARS-CoV-2 viral RNA
300 loads were determined using Droplet Digital PCR (ddPCR) supermix for probes without dUTP
301 (Bio-Rad Laboratories Ltd.) and the QX200 Droplet Digital PCR System Workflow (Bio-Rad
302 Laboratories Ltd.). The ddPCR primers and probes were previously reported⁴⁶.

303 ***Multiplex cytokines quantification.*** Cytokines in mouse lung homogenates were measured
304 using a custom ProcartaPlex™ Mouse Mix & Match Panels kit (Invitrogen, Waltham, MA, USA)
305 on the Bio-Plex 200 (Bio-Rad Laboratories Ltd.).

306 ***Histological analysis.*** For each group analyzed (N=5 mice/group), the right lung lobe was
307 extracted, fixed in formalin and paraffin embedded as described⁴⁵. Lung sections were stained
308 with Carstairs staining for histological analysis. Prior to conduct immunofluorescence assay,

309 lung sections were deparaffined, hydrated then heat-induced epitope retrieval 16h at 60°C with
310 Diva Decloaker solution (Biocare Medical, Pacheco, CA, USA). Immunostainings were
311 performed to detect SARS-CoV-2 N antigen and leukocyte infiltration using 20µg/mL rabbit anti-
312 N (Rockland chemicals, Limerick, PA, USA)/anti-rabbit IgG Alexa 488 (Jackson Immuno
313 Research lab, West Grove, PA, USA) and 10µg/mL biotinylated anti-CD45 antibodies (BD
314 Bioscience, Franklin Lakes, NJ, USA)/anti Rat IgG Alexa Plus 647 (Thermo Fisher Scientific,
315 Waltham, MA, USA). Slide were imaged using Axioscan 7 instrument (Carl Zeiss Microscopy,
316 New York, USA) then black and white adjustment were performed with Zen lite 3.7 (Carl Zeiss
317 Microscopy). Quantification of positive area signal for N and CD45 staining were performed
318 using Fiji (ImageJ) threshold analyse tools.

319 ***Illumina viral sequencing.*** RNA extracts were processed for reverse transcription ([step a](#)) and
320 targeted SARS-CoV-2 amplification using the ARTIC V3 or V4.1 primer scheme
321 (<https://github.com/artic-network/primer-schemes/tree/master/nCoV-2019>) ([step b](#)). Samples
322 were purified ([step b](#)) and Nextera DNA Flex library preparation ([step c](#)) was performed for
323 Illumina PE150 paired-end amplicon sequencing on a NovaSeq or MiSeq instrument at the
324 McGill Genome Centre using best practices. Each sample was sequenced twice on different
325 days to obtain a target of minimum 10 million reads per sample. The detailed protocols can be
326 accessed with the following links.

327 Step a: [dx.doi.org/10.17504/protocols.io.bjgekjte](https://doi.org/10.17504/protocols.io.bjgekjte).

328 Step b: [dx.doi.org/10.17504/protocols.io.ewov18e4ygr2/v2](https://doi.org/10.17504/protocols.io.ewov18e4ygr2/v2).

329 Step c: [dx.doi.org/10.17504/protocols.io.bjgnkjve](https://doi.org/10.17504/protocols.io.bjgnkjve).

330 ***Nanopore viral sequencing.*** RNA extracts were processed by reverse transcription with
331 Lunascript⁴⁷. Targeted SARS-COV-2 amplification was performed using five of the 29 Midnight
332 primers⁴⁸. We targeted the 4167 to 5359 bp region with the primer pairs SARSCoV_1200_5. To

333 target the Spike region we used primers pairs SARSCoV_1200_23, SARSCoV_1200_25
334 SARSCoV_1200_22 and SARSCoV_1200_24. Amplification of the primers was performed
335 following Freed and Silander protocol⁴⁹. Nanopore library preparation was made following
336 Reiling *et al.* 2020 and libraries were sequenced on the PromethION 24 sequencer with
337 PromethION Flow Cells V.9.4.1 for a total of 10 million reads⁵⁰.

338 **Genome data processing.** Following sequencing, the reads from each sample were used to
339 call variants using Freebayes v1.3.6⁵¹ and the results were saved as a VCF file which was used
340 to compare genomic variation across passages. Others have called variants with other tools
341 such as DeepSNV²⁴ and VarScan⁵². DeepSNV was not used as it only investigates SNVs⁵³,
342 when indels have been found to confer selective advantages⁵⁴. Freebayes has been observed
343 to perform slightly superiorly than VarScan when calling variants in wastewater samples⁵⁵ and
344 in internal benchmarking (data not shown). The process is described briefly as follows: first, the
345 raw reads from each sample were aligned with BWA MEM v0.7.17⁵⁶ to the reference strain
346 genome sequence (NC_045512.2). The resulting alignments were sorted with duplicate reads
347 flagged. The minimum number of aligned reads for each was logged, and each sample was
348 again aligned and processed, then randomly down sampled to match this minimum number of
349 reads. The minimum number of reads per sample in the first part of the study across passage 0
350 (P0) and P10 was 8,812,604. The minimum number of reads per sample in the second part of
351 the study across P13, P17, and P20 was 34,253,784. All variants with a quality of less than 20
352 or a depth below 10 were removed from the analysis. Any variant alleles that overlapped with
353 ARTIC sequencing primers were also removed. Merged VCF files, representing the combination
354 of reads across two sequencing batches for each sample, were used for the paper's main
355 results.

356 Nanopore reads were processed similarly using freebayes, although run a second time using
357 freebayes with the haplotype-basis-alleles option to use statistical priors to further remove noise

358 from reads. Given that Nanopore was used to validate Illumina calls and evaluate for co-
359 inheritance, its raw output was not down sampled. Its raw output was aligned using minimap2
360 v2.24, then processed identically to Illumina reads.

361 **Variant annotation.** Every variant allele was inputted into COVID-19 Ensembl variant effect
362 predictor (VEP) (<https://covid-19.ensembl.org/index.html>) to determine functional consequences
363 and the involved gene and amino acid change⁵⁷. Variants whose VAF changed at least once
364 across passages during the study were logged and input to the UCSC Genome Browser
365 (<https://genome.ucsc.edu/>), checking for annotations of antibody escape, CD8 escape, vaccine
366 targets, drug resistance, or variants of concern²⁶.

367 **Determination of spike allele co-inheritance.** Alleles were determined to be co-inherited if the
368 nanopore, statistically derived allele frequency was identical for multiple alleles in the same
369 passage.

370 **Antibody neutralization studies.** Sera from twenty-four healthy vaccinated (3x) individuals
371 were analyzed for neutralizing activity against Wuhan-like, and Beta and Delta P0 and P20
372 viruses. Serially diluted sera (in quadruplicate) were incubated with 100 TCID₅₀ of virus for 1 h
373 at 37°C before addition to Vero E6 cells. Three days later, the 96-well plates were observed
374 using an inverted microscope for signs of infection. Neutralization titers were determined and
375 defined as the highest serum dilution preventing infection.

376 **Ethics.** The study was conducted in accordance with the Declaration of Helsinki, and mouse
377 protocols were approved by the Comité de protection des animaux de l'Université Laval. Our
378 IRB determined that our work did not constitute gain-of-function research as virus was
379 unmodified and represented circulating variants with the study conducted without experimental
380 selective pressures. Sera obtained from humans were procured following ERB approval (ERB
381 #2022-6204).

382 **Statistics and reproducibility.** All statistical analyses were conducted using R/4.2.1. All
383 statistical comparisons between passages were corrected for multiple testing using a Benjamini-
384 Hochberg p-value adjustment. Statistical tests included unpaired and paired t-tests and Mann-
385 Whitney tests, as noted in figures. Reproducibility is described in each method.

386 **Source code.** All code used in this study, from sample processing to data analysis, are publicly
387 available on Github at the following link:

388 https://github.com/juliandwillett/SARS_CoV_2_Serial_Passaging_Study.

389 **Data availability.** VCF files used to complete computational analyses are available by
390 reasonable request.

391

392 **Declarations:**

393 **Competing interest.**

394 All authors declare no competing interests.

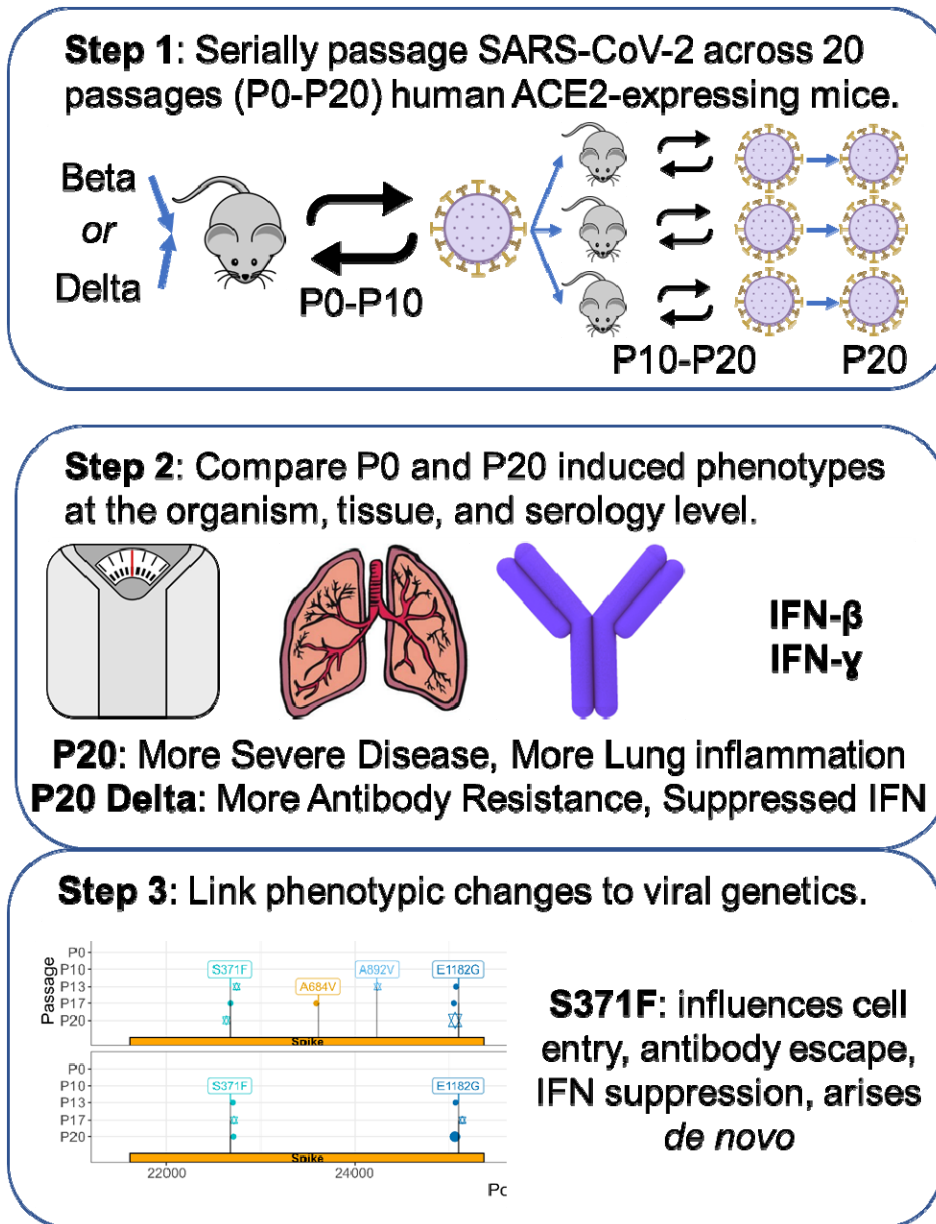
395 **Authors contributions.** Julian Daniel Sunday Willett conceived of the computational analyses
396 needed for this study, completed all computational analysis of viral sequencing data, and wrote
397 the majority of the manuscript. Louis Flamand and Jiannis Ragoussis conceived of the study.
398 Louis Flamand contributed to manuscript revisions, wrote sections relevant to animal models
399 and antibody neutralization studies and performed analysis of results. Jiannis Ragoussis
400 supervised sequencing data generation and analysis. Isabelle Dubuc and Leslie Gudimard
401 performed all works involving live SARS-CoV-2 viruses. Annie Gravel participated in the
402 sequence analysis and methodological design of experiments. Ana Claudia dos Santos Pereira
403 Andrade performed the Luminex assay and analyzed the data. Émile Lacasse performed the
404 immunohistological analyses and analyzed the data. Paul Fortin provided key reagents. Jose

405 Hector Galvez contributed bioinformatics analysis review and manuscript revisions. Ju-Ling Liu,
406 Jose Avila Cervantes, Haig Hugo Vrej Djambazian, Anne-Marie Roy, Sally Lee and Shu-Huang
407 Chen supported the SARS-CoV-2 viral sequencing.

408 ***Acknowledgments.***

409 This research was enabled in part by support provided by Calcul Québec (calculquebec.ca) and
410 the Digital Research Alliance of Canada (alliancecan.ca). This study was supported by the
411 Canadian Institutes for Health Research (CIHR 476575) to JDSW, a CIHR operating grant to
412 the Coronavirus Variants Rapid Response Network (CoVaRR-Net) to LF and JR and CIHR
413 grant (GA1-117694) to LF. The funding body had no role in the design of the study or collection,
414 analysis, interpretation, or reporting of the data. We thank Ines Colmegna for providing
415 vaccinated patient sera. We thank Silvia Vidal for her guidance regarding SARS-CoV-2
416 evolutionary mechanisms. ChatGPT was used to decrease the word count in the abstract with
417 output carefully examined for representing our results. We thank Dr Serge Rivest's imagery
418 platform for the slide scanning service.

419 **Figures**



420

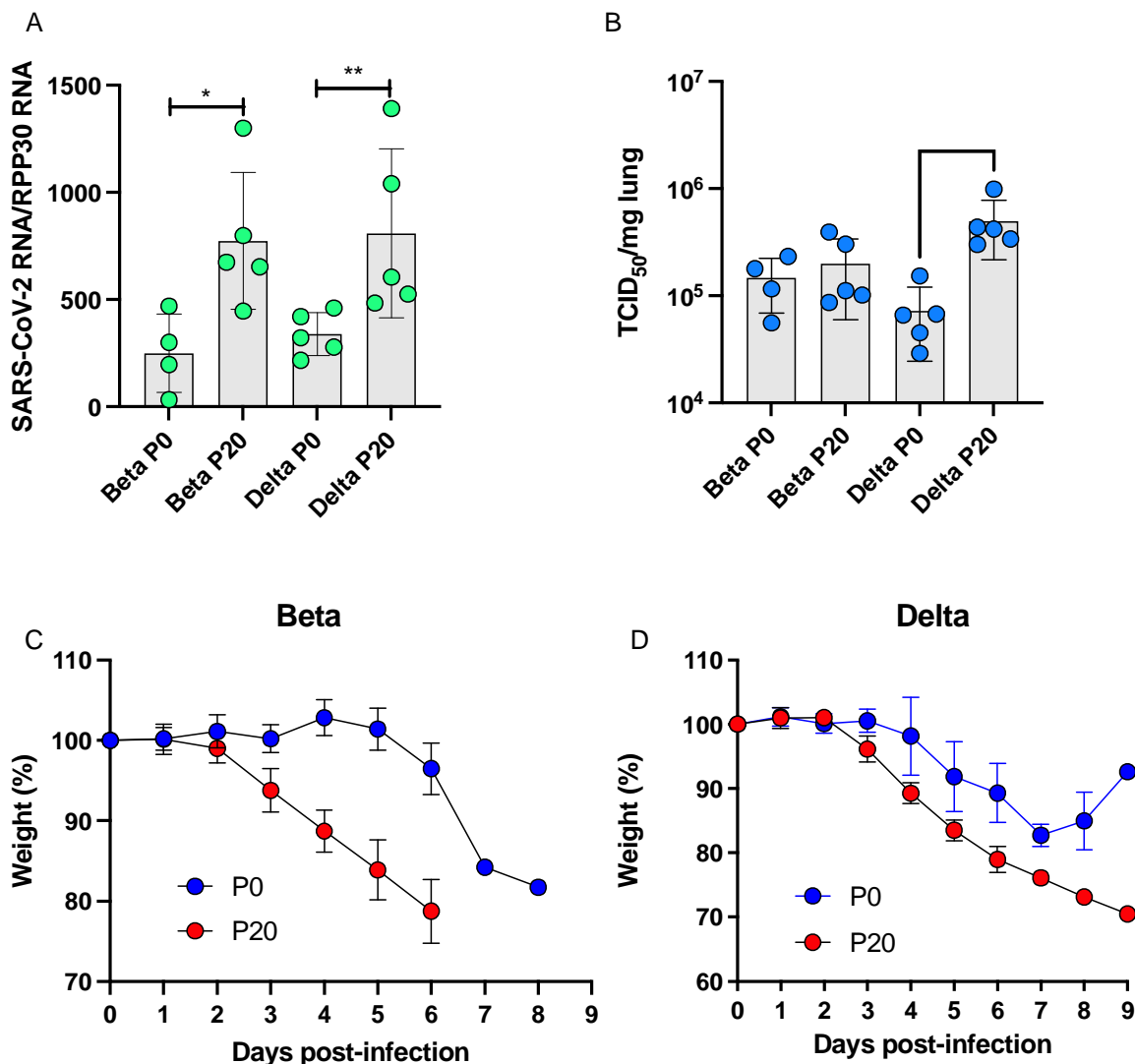
421

422

423 **Figure 1. Study design.** SARS-CoV-2 ACE2-adapted mice were inoculated with either B.1.351
424 (Beta) or B.1.617.2 (Delta) virus and left for three days for virus to proliferate. They were then
425 sacrificed with the lung homogenate used to infect another mouse. This was repeated for ten
426 passages. P10 virus for each lineage was then used to infect three additional mice and the
427 process was repeated for an additional ten passages. P0 and P20 virus for each lineage was
428 subsequently used to infect additional mice to compare weight loss and survival between early

429 and late passage virus, and test non-adapted mouse susceptibility to the virus. Antibody
430 neutralization of virus was also compared.

431



432

433 **Figure 2. Pathogenesis of P0 and P20 viruses in K18-ACE2 mice.** Mice (n = 15/group) were

434 infected with 500 TCID₅₀ of P0 or P20 Beta and Delta viruses. (A-B) On day 3 post-infection,

435 mice (n = 5) were euthanized and lungs collected for SARS-CoV-2 RNA (A) and infectious viral

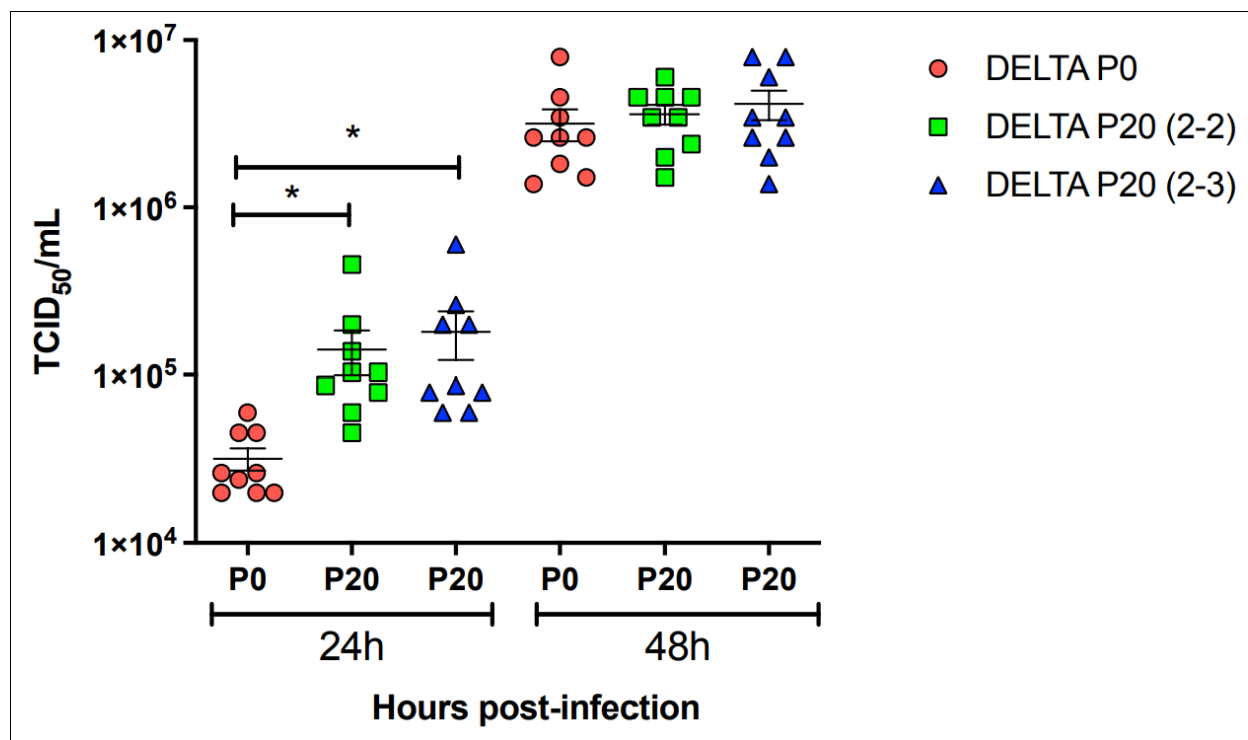
436 load (B) determination. Results are expressed as mean ± SD SARS-CoV-2 RNA copies/RPP30

437 RNA copies (A) and mean ± SD SARS-CoV-2 TCID₅₀/mg of lung tissue (B). (C-D) The weight of

438 each mouse (n = 10/group) was monitored daily throughout the experiment and reported as

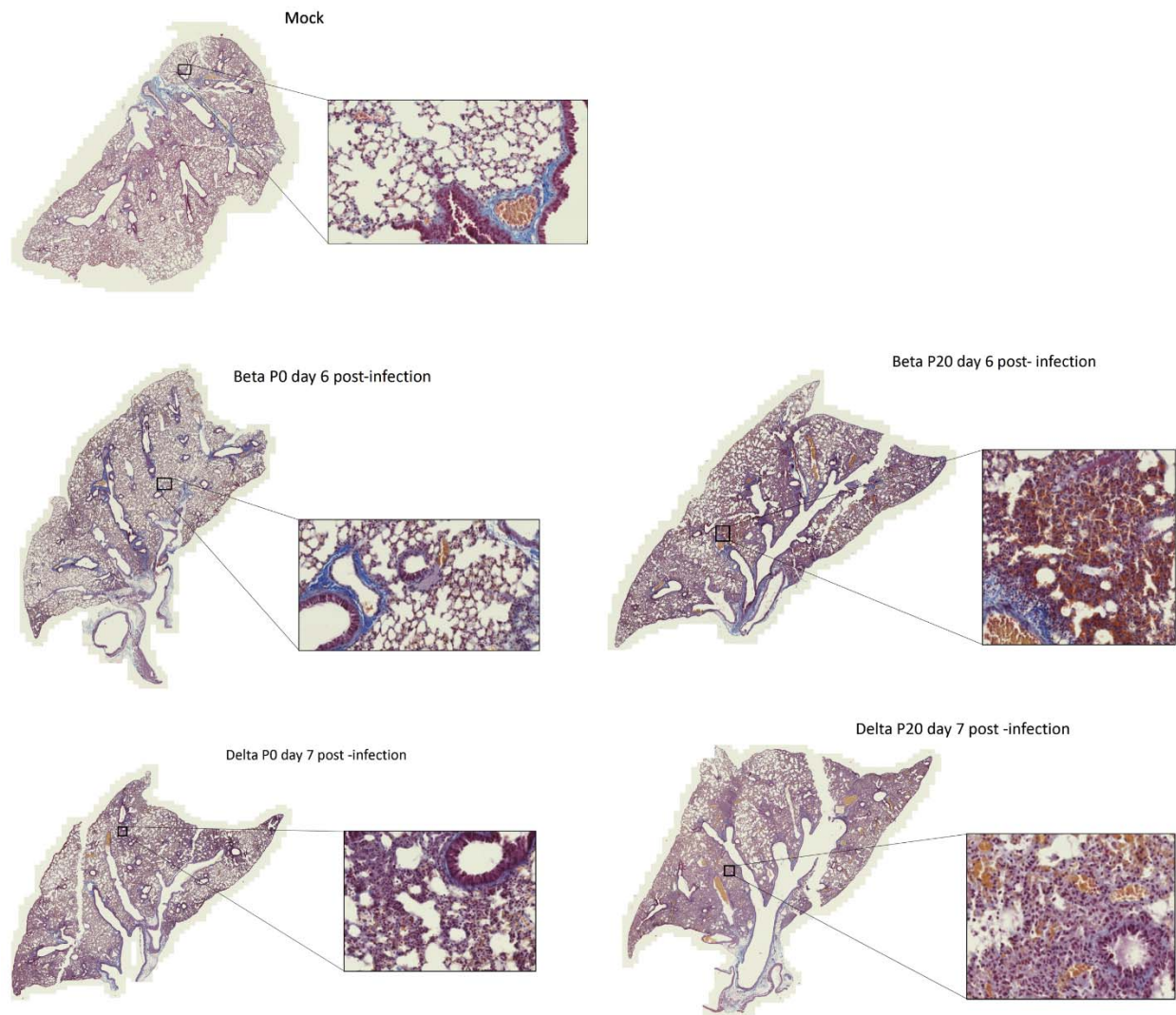
439 mean percentage ± SD of weight relative to day 0. * ≤ 0.05 and **: p ≤ 0.008 as determined

440 using non-parametric Mann-Whitney test.



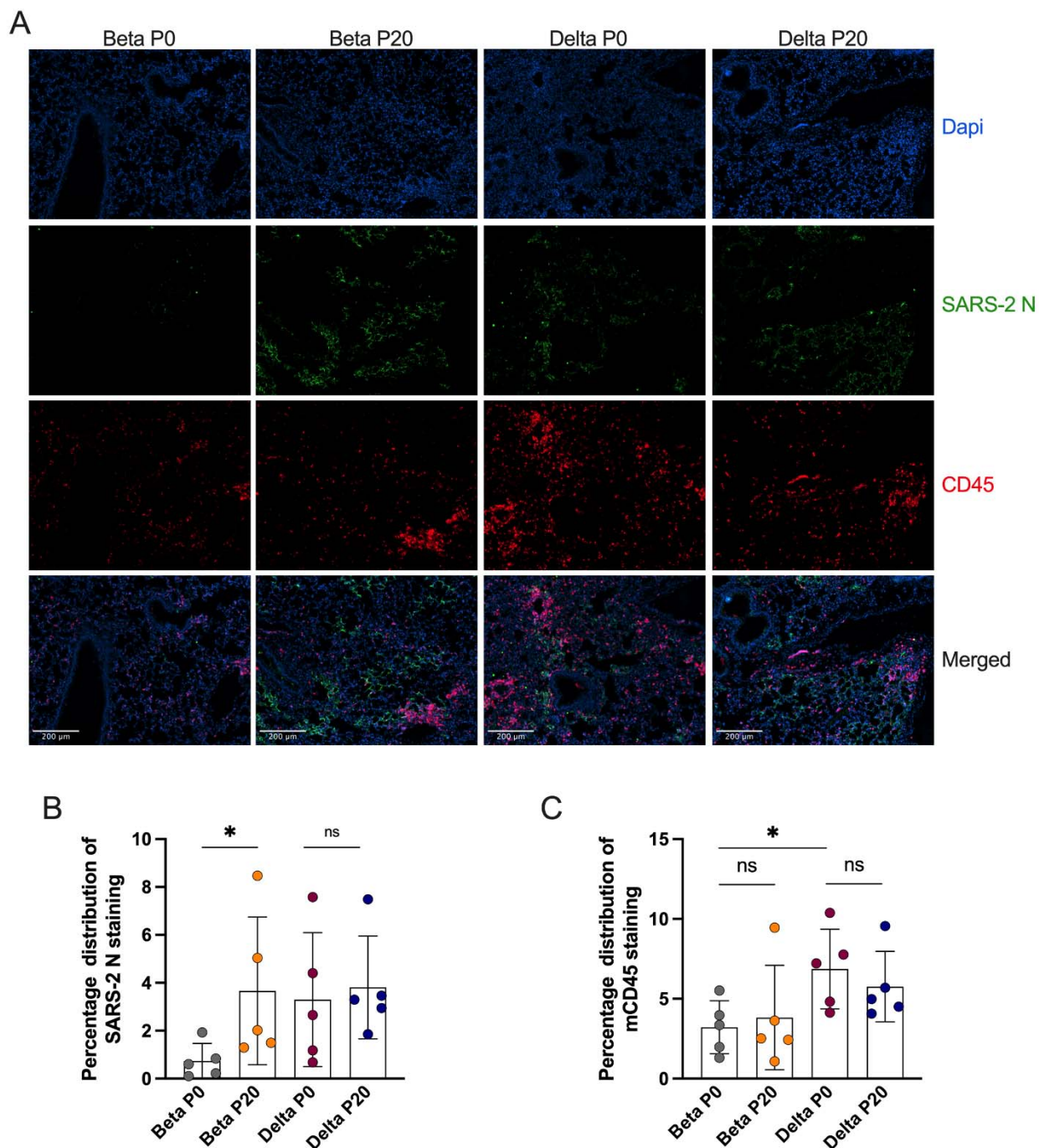
441 **Figure 3. Growth kinetics of P0 and P20 Delta viruses.** P0 and two independently evolved
442 P20 Delta viruses were used to infect Vero cells at a multiplicity of infection of 0.005. Cell-free
443 supernatants were collected at 24 h and 48 h and used for viral titration. Results are expressed
444 as mean ± SD TCID₅₀/mL. *: p=0.02 as determined using an unpaired t-test.

445



446
447 **Figure 4.** Lung histology of mice infected with Beta and Delta P0 and P20 viruses. Mice were
448 mock-infected (A) or infected with 500 TCID₅₀ of Beta P0 (B), Beta P20 (C), Delta P0 (D) of
449 Delta P20 viruses. Lungs were harvested on day 6 (Beta) or day 7 (Delta) post infection,
450 formalin fixed and processed for Carstairs staining.

451



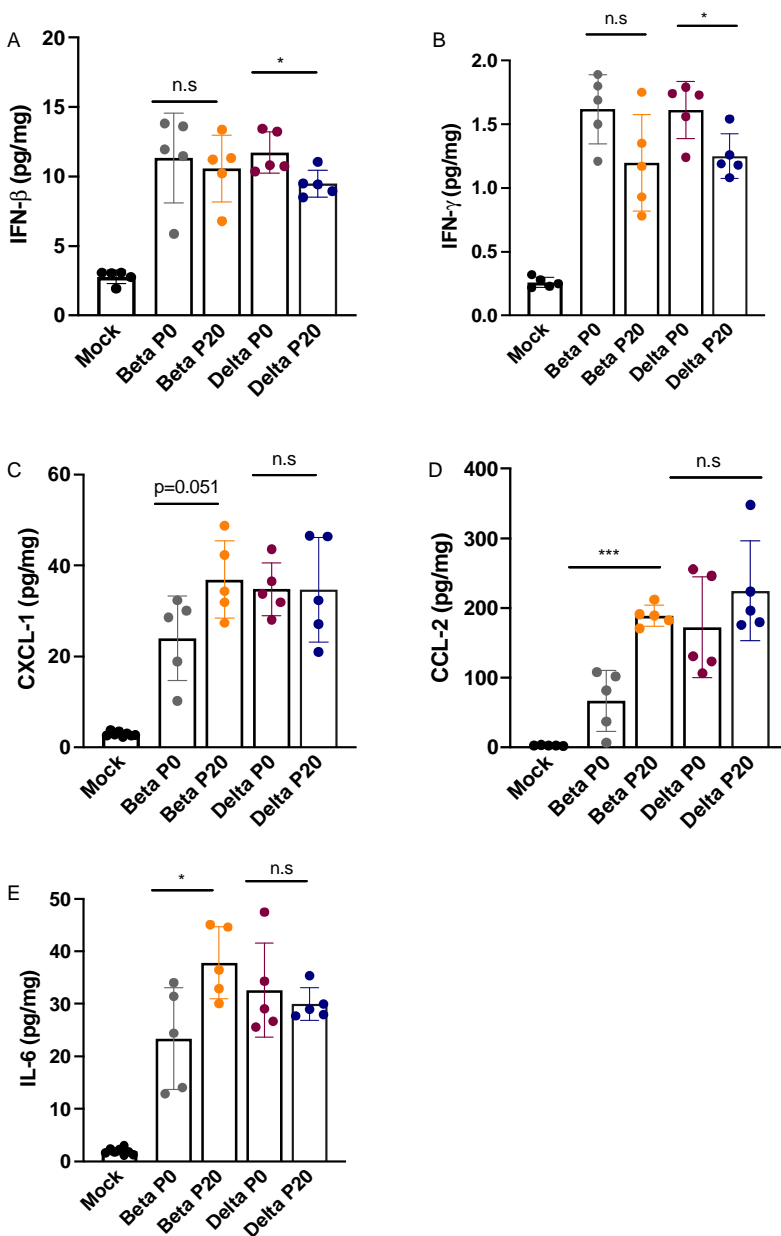
452
453 **Figure 5.** Immunohistological staining of mouse lungs infected with Beta and Delta P0 and P20
454 viruses. (A) Infected lung tissues were stained with DAPI (blue/nuclei), anti-SARS CoV-2
455 nucleocapsid (N) protein (green), anti-mouse CD45 (red). (B) Graphical (mean +/-SD)
456 representation of SARS CoV-2 N (B) or CD45 (C) staining. Each dot represents data collected

457 from one section of lung tissue from one mouse. Entire lung sections were imaged with

458 representative images shown. * $p < 0.05$ and N.S determined using Mann-Whitney test.

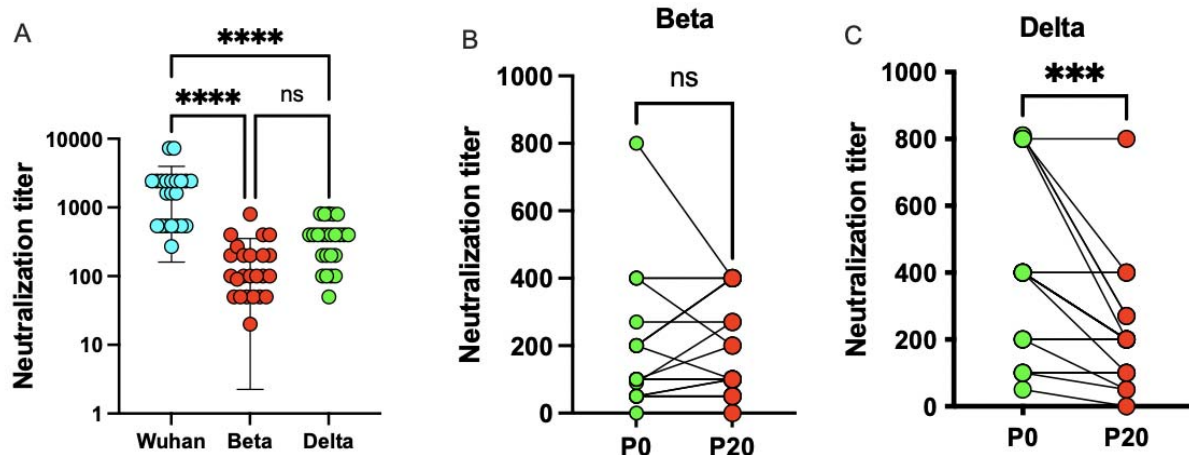
459

460



461

462 **Figure 6.** Monitoring of cytokines in lungs of mice infected with Beta and Delta P0 and P20
463 viruses. K18-ACE2 mice were mock-infected or infected with 500 TCID₅₀ of Beta P0, Beta P20
464 Delta P0 and Delta P20 viruses. On day 3 post-infection, mice were euthanized, lungs were
465 harvested and homogenized. The cytokine content in the homogenates were determines using
466 the Luninex assay. *p<0.05, ***p<0.005 as determined using either unpaired t-test (A, D, E) or
467 Mann-Whitney test (B).



468

469 **Figure 7. Neutralization of P0 and P20 viruses with sera from vaccinated subjects. (A)**

470 Neutralization assay of Wuhan-like, Beta, and Delta viruses using sera from 24 vaccinated

471 subjects. Individual results and mean \pm SD neutralization titer against different SARS-CoV-2

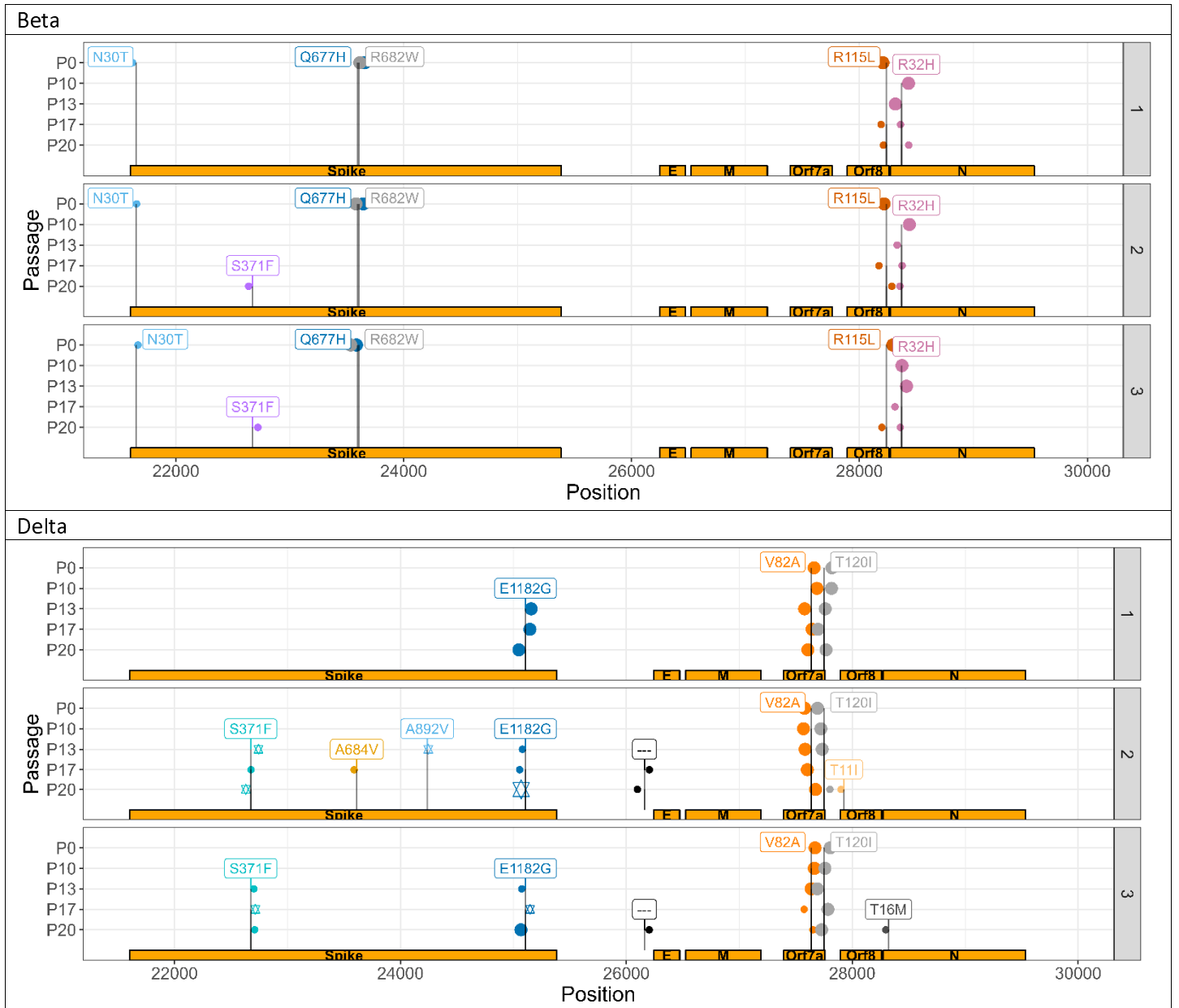
472 isolates are presented. ****: $p < 0.0001$ determined using one way-ANOVA. ns: not statistically

473 significant. (B) Pair-wise comparison of the sera used in A in neutralization assay against P0

474 and P20 Beta viruses. (C) Pair-wise comparison of the sera used in A in neutralization assay

475 against P0 and P20 Delta viruses. ***: $p > 0.002$ determined using paired t-test.

476



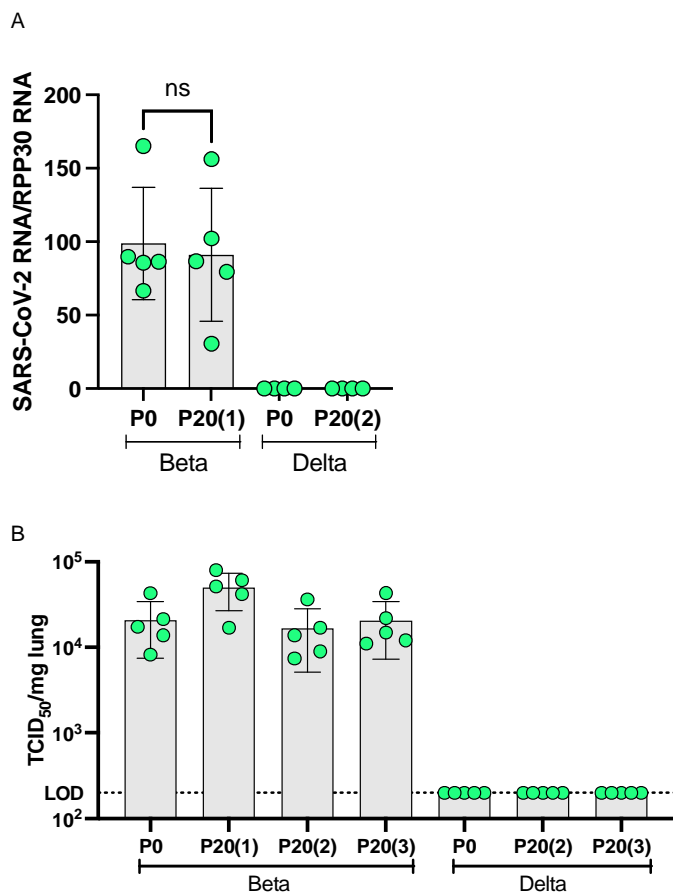
477 **Figure 8. More variant alleles of clinical relevance arose de novo and persisted in spike**
 478 **for Delta lineage compared to Beta, with key variants being co-inherited.** Each line and
 479 sample number refers to a select viral sample being passaged. P0 and P10 are identical across
 480 samples, given that it was passaged in a single animal up to P10. VAF: variant allele frequency.
 481 P refers to passage. Variant allele incidence by sample in Delta lineage virus. Larger points
 482 represent variant alleles with a within-sample, Illumina-derived allele-frequency of 1.0, smaller

483 ones 0.5. Stars in a given passage represent alleles that are likely co-inherited per Nanopore
484 sequencing.

486 **Table 1. Annotations of select variants that changed in frequency across the study.**

Variant	Amino Acid Change	Annotation	Interacting Human Protein	Human protein implicated with COVID-19 severity or susceptibility
A929G	ORF1ab I222V, nsp2	Protein interacting*	GIGYF2, FKBP15* , WASHC4, RAP1GDS1, POR, eIF4E2* , SLC27A2	GIGYF2 (PMID 35878012)
C22674T	Spike S371F	Protein interacting, antibody escape, vaccine target, Omicron-associated variant allele ²⁶	GOLGA7, ZDHHC5	GOLGA7 (PMID 34961524), ZDHHC5 (PMID 34961524)
A25107G	Spike E1182G	Protein interacting, vaccine target	GOLGA7, ZDHHC5	GOLGA7 (PMID 34961524), ZDHHC5 (PMID 34961524)
G28237T	ORF8 R115L	Protein interacting*	COL6A1, PCSK6, LOX* , DNMT1* , NPC2, CISD3, ITGB1, PLAT, STC2, TOR1A, PLOD2* , INHBE, CHPF2, UGGT2, FBXL12, PLEKHF2, SMOC1, POFUT1, FKBP10* , ERLEC1, IL17RA, ADAMTS1, HS6ST2, SDF2, NEU1, GDF15, TM2D3, SIL1, EDEM3, ERP44, PVR, NGLY1, OS9, ADAM9, NPTX1, POGLUT2, POGLUT3, ERO1B, PLD3, FOXRED2, CHPF, PUSL1, HYOU1, MFGE8, FKBP7, GGH, EMC1	COL6A1 (PMID 35468151), LOX (PMID 34616409), PLAT (PMID 34786557), PLOD2 (PMID 33328453), FBXL12 (PMID 34183789), FKBP10 (PMID 35571107), IL17RA (PMID 33723527), HS6ST2 (PMID 32970989), NEU1 (PMID 36714013), GDF15 (PMID 35251002), ADAM9 (PMID 34698500), PLD3 (PMID 36182629)

487 **Supplemental Figures**



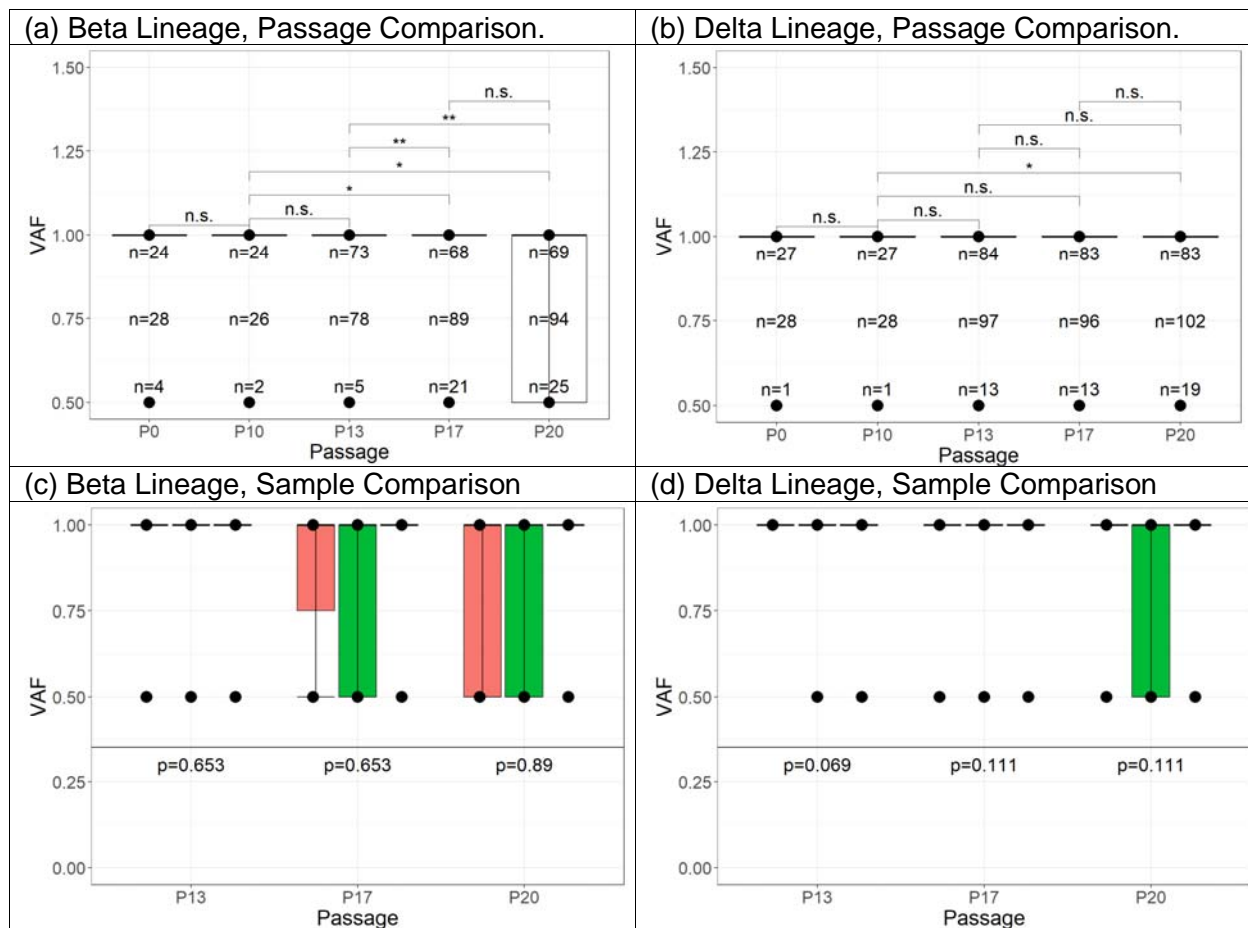
488

489 **Supplementary Figure 1. Infection of C57BL6 mice with P0 and P20 Beta and Delta**

490 **viruses.** Mice (n = 5/group) were infected intranasally with 3000 TCID₅₀ of P0 and P20 Beta
491 and Delta viruses. On the third day post infection, mice were euthanized and lungs collected for
492 RNA extraction and infectious viral load determination. A) Mean +/- SD of normalized SARS-
493 CoV-2 RNA copies as determined using ddPCR. B) Mean TCID₅₀/mg of lung. LOD=limit of
494 detection.

495

496



497 **Supplemental Figure 2. Boxplots of variant allele frequency by (a-b) passage and (c-d)**

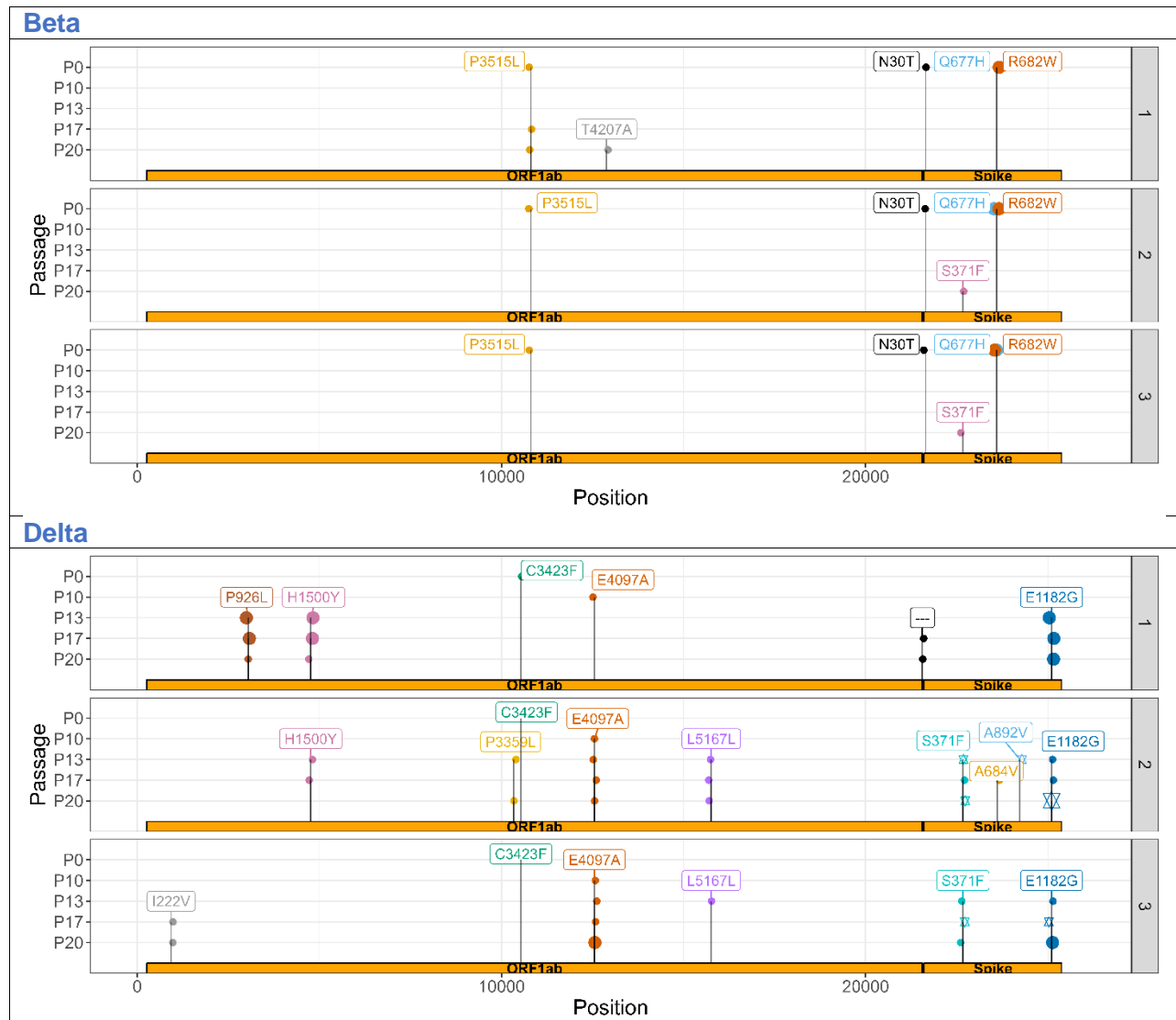
498 **sample.** Each N refers to the number of variant alleles for each MAF and in total against the

499 NC_045512.2 reference sequence. Single samples were sequenced for P0 and P10 with three

500 samples from P13, P17, and P20. Box fill in (c-d) signifies sample number. For significance,

501 n.s.: adjusted p-value > 0.05, *: adjusted p-value > 0.01, **: adjusted p-value ≤ 0.01, using

502 unpaired t-tests.



503 **Supplemental Figure 3. More novel, high confidence, non-synonymous, changing alleles**
 504 **appeared in Delta versus Beta in the ORF1ab coding region.** VAF: variant allele frequency.
 505 P refers to passage. Variant allele incidence by sample in Delta lineage virus. Larger points
 506 represent variant alleles with a within-sample, Illumina-derived allele-frequency of 1.0, smaller
 507 ones 0.5. Stars in a given passage represent alleles that are likely co-inherited per Nanopore
 508 sequencing.

509

510 **Supplemental Table 1. Table of variant alleles that changed MAF during the study,**
511 **alongside their annotations. Available in “Supplemental Tables.csv”.**

512 **References:**

- 513 1. Jacobs, J.L., Haidar, G. & Mellors, J.W. COVID-19: Challenges of Viral Variants. *Annu Rev Med*
514 (2022).
- 515 2. V'Kovski, P., Kratzel, A., Steiner, S., Stalder, H. & Thiel, V. Coronavirus biology and replication:
516 implications for SARS-CoV-2. *Nat Rev Microbiol* **19**, 155-170 (2021).
- 517 3. Sun, F. *et al.* SARS-CoV-2 Quasispecies Provides an Advantage Mutation Pool for the Epidemic
518 Variants. *Microbiol Spectr* **9**, e0026121 (2021).
- 519 4. Velavan, T.P. *et al.* Host genetic factors determining COVID-19 susceptibility and severity.
520 *EBioMedicine* **72**, 103629 (2021).
- 521 5. Belsky, J.A. *et al.* COVID-19 in immunocompromised patients: A systematic review of cancer,
522 hematopoietic cell and solid organ transplant patients. *J Infect* **82**, 329-338 (2021).
- 523 6. Van Cleemput, J. *et al.* Organ-specific genome diversity of replication-competent SARS-CoV-2.
524 *Nat Commun* **12**, 6612 (2021).
- 525 7. Wang, R., Chen, J. & Wei, G.W. Mechanisms of SARS-CoV-2 Evolution Revealing Vaccine-
526 Resistant Mutations in Europe and America. *J Phys Chem Lett* **12**, 11850-11857 (2021).
- 527 8. Liu, Y. *et al.* The N501Y spike substitution enhances SARS-CoV-2 infection and transmission.
528 *Nature* **602**, 294-299 (2022).
- 529 9. Motozono, C. *et al.* SARS-CoV-2 spike L452R variant evades cellular immunity and increases
530 infectivity. *Cell Host Microbe* **29**, 1124-1136 e11 (2021).
- 531 10. Cherian, S. *et al.* SARS-CoV-2 Spike Mutations, L452R, T478K, E484Q and P681R, in the Second
532 Wave of COVID-19 in Maharashtra, India. *Microorganisms* **9**(2021).
- 533 11. Liu, Y. *et al.* Delta spike P681R mutation enhances SARS-CoV-2 fitness over Alpha variant. *Cell*
534 *Rep* **39**, 110829 (2022).
- 535 12. Planas, D. *et al.* Reduced sensitivity of SARS-CoV-2 variant Delta to antibody neutralization.
536 *Nature* **596**, 276-280 (2021).
- 537 13. Gu, H. *et al.* Adaptation of SARS-CoV-2 in BALB/c mice for testing vaccine efficacy. *Science* **369**,
538 1603-1607 (2020).
- 539 14. Wasik, B.R. *et al.* Influenza Viruses in Mice: Deep Sequencing Analysis of Serial Passage and
540 Effects of Sialic Acid Structural Variation. *J Virol* **93**(2019).
- 541 15. Sun, S. *et al.* Characterization and structural basis of a lethal mouse-adapted SARS-CoV-2. *Nat*
542 *Commun* **12**, 5654 (2021).
- 543 16. Huang, K. *et al.* Q493K and Q498H substitutions in Spike promote adaptation of SARS-CoV-2 in
544 mice. *EBioMedicine* **67**, 103381 (2021).
- 545 17. Chung, H., Noh, J.Y., Koo, B.S., Hong, J.J. & Kim, H.K. SARS-CoV-2 mutations acquired during
546 serial passage in human cell lines are consistent with several of those found in recent natural
547 SARS-CoV-2 variants. *Comput Struct Biotechnol J* **20**, 1925-1934 (2022).
- 548 18. Sonnleitner, S.T. *et al.* The mutational dynamics of the SARS-CoV-2 virus in serial passages in
549 vitro. *Viol Sin* **37**, 198-207 (2022).
- 550 19. Khalil, B.A., Elemam, N.M. & Maghazachi, A.A. Chemokines and chemokine receptors during
551 COVID-19 infection. *Comput Struct Biotechnol J* **19**, 976-988 (2021).
- 552 20. Gadotti, A.C. *et al.* IFN-gamma is an independent risk factor associated with mortality in patients
553 with moderate and severe COVID-19 infection. *Virus Res* **289**, 198171 (2020).
- 554 21. Berri, F. *et al.* Early plasma interferon-beta levels as a predictive marker of COVID-19 severe
555 clinical events in adult patients. *J Med Virol* **95**, e28361 (2023).
- 556 22. Tada, T. *et al.* Convalescent-Phase Sera and Vaccine-Elicited Antibodies Largely Maintain
557 Neutralizing Titer against Global SARS-CoV-2 Variant Spikes. *mBio* **12**, e0069621 (2021).

- 558 23. Dupont, L. *et al.* Neutralizing antibody activity in convalescent sera from infection in humans
559 with SARS-CoV-2 and variants of concern. *Nat Microbiol* **6**, 1433-1442 (2021).
- 560 24. Tonkin-Hill, G. *et al.* Patterns of within-host genetic diversity in SARS-CoV-2. *Elife* **10**(2021).
- 561 25. Turakhia, Y. *et al.* Pandemic-scale phylogenomics reveals the SARS-CoV-2 recombination
562 landscape. *Nature* **609**, 994-997 (2022).
- 563 26. Kent, W.J. *et al.* The human genome browser at UCSC. *Genome Res* **12**, 996-1006 (2002).
- 564 27. Zeng, X.T., Yu, X.X. & Cheng, W. The interactions of ZDHHC5/GOLGA7 with SARS-CoV-2 spike (S)
565 protein and their effects on S protein's subcellular localization, palmitoylation and pseudovirus
566 entry. *Virology* **18**, 257 (2021).
- 567 28. Wu, Z. *et al.* Palmitoylation of SARS-CoV-2 S protein is essential for viral infectivity. *Signal*
568 *Transduct Target Ther* **6**, 231 (2021).
- 569 29. Zhang, Y., Qin, Z., Sun, W., Chu, F. & Zhou, F. Function of Protein S-Palmitoylation in Immunity
570 and Immune-Related Diseases. *Front Immunol* **12**, 661202 (2021).
- 571 30. Cao, Y. *et al.* BA.2.12.1, BA.4 and BA.5 escape antibodies elicited by Omicron infection. *Nature*
572 **608**, 593-602 (2022).
- 573 31. Xu, Z. *et al.* SARS-CoV-2 impairs interferon production via NSP2-induced repression of mRNA
574 translation. *Proc Natl Acad Sci U S A* **119**, e2204539119 (2022).
- 575 32. Song, L. *et al.* The main protease of SARS-CoV-2 cleaves histone deacetylases and DCP1A,
576 attenuating the immune defense of the interferon-stimulated genes. *J Biol Chem* **299**, 102990
577 (2023).
- 578 33. Stelzer, G. *et al.* The GeneCards Suite: From Gene Data Mining to Disease Genome Sequence
579 Analyses. *Curr Protoc Bioinformatics* **54**, 1 30 1-1 30 33 (2016).
- 580 34. Combadiere, B. *et al.* LOX-1-Expressing Immature Neutrophils Identify Critically-Ill COVID-19
581 Patients at Risk of Thrombotic Complications. *Front Immunol* **12**, 752612 (2021).
- 582 35. Pietzner, M. *et al.* Genetic architecture of host proteins involved in SARS-CoV-2 infection. *Nat*
583 *Commun* **11**, 6397 (2020).
- 584 36. Wang, S. *et al.* Network Pharmacology and Bioinformatics Analyses Identify Intersection Genes
585 of Vitamin D3 and COVID-19 as Potential Therapeutic Targets. *Front Pharmacol* **13**, 874637
586 (2022).
- 587 37. Staab-Weijnitz, C.A. *et al.* FK506-Binding Protein 10, a Potential Novel Drug Target for Idiopathic
588 Pulmonary Fibrosis. *Am J Respir Crit Care Med* **192**, 455-67 (2015).
- 589 38. Johnson, B.A. *et al.* Loss of furin cleavage site attenuates SARS-CoV-2 pathogenesis. *Nature* **591**,
590 293-299 (2021).
- 591 39. Rahimi, F. & Talebi Bezmin Abadi, A. Implications of the Emergence of a New Variant of SARS-
592 CoV-2, VUI-202012/01. *Arch Med Res* **52**, 569-571 (2021).
- 593 40. Tarres-Freixas, F. *et al.* Heterogeneous Infectivity and Pathogenesis of SARS-CoV-2 Variants Beta,
594 Delta and Omicron in Transgenic K18-hACE2 and Wildtype Mice. *Front Microbiol* **13**, 840757
595 (2022).
- 596 41. Zeng, C. *et al.* Neutralization of SARS-CoV-2 Variants of Concern Harboring Q677H. *mBio* **12**,
597 e0251021 (2021).
- 598 42. Sui, Y., Li, J., Venzon, D.J. & Berzofsky, J.A. SARS-CoV-2 Spike Protein Suppresses ACE2 and Type I
599 Interferon Expression in Primary Cells From Macaque Lung Bronchoalveolar Lavage. *Front*
600 *Immunol* **12**, 658428 (2021).
- 601 43. Kim, K. *et al.* The roles of APOBEC-mediated RNA editing in SARS-CoV-2 mutations, replication
602 and fitness. *Sci Rep* **12**, 14972 (2022).
- 603 44. Lei, C., Yang, J., Hu, J. & Sun, X. On the Calculation of TCID₅₀ for Quantitation of Virus
604 Infectivity. *Virology* **36**, 141-144 (2021).

- 605 45. Dubuc, I. *et al.* Cytokines and Lipid Mediators of Inflammation in Lungs of SARS-CoV-2 Infected
606 Mice. *Front Immunol* **13**, 893792 (2022).
- 607 46. Lacasse, E. *et al.* SARS-CoV-2 Nsp2 Contributes to Inflammation by Activating NF-kappaB. *Viruses*
608 **15**(2023).
- 609 47. Chen, S.-H., J Reiling, S., Quick, J. & Ragoussis, I. Artic nCoV-2019 McGill modified Lunascript
610 Reverse Transcriptase sequencing protocol. *Protocols.io* (2020).
- 611 48. Freed, N.E., Vlkova, M., Faisal, M.B. & Silander, O.K. Rapid and inexpensive whole-genome
612 sequencing of SARS-CoV-2 using 1200 bp tiled amplicons and Oxford Nanopore Rapid Barcoding.
613 *Biol Methods Protoc* **5**, bpaa014 (2020).
- 614 49. Freed, N. & Silander, O. SARS-CoV2 genome sequencing protocol (1200bp amplicon "midnight"
615 primer set, using Nanopore Rapid kit) V.6. *Protocols.io* (2021).
- 616 50. J Reiling, S., Roy, A.-M., Chen, S.-H. & Ragoussis, I. nCoV-2019 McGill Nanopore LibPrep Protocol,
617 10 ng NB. *Protocols.io* (2020).
- 618 51. Garrison, E.P.M.G. Haplotype-based variant detection from short-read sequencing. *arXiv* (2012).
- 619 52. N'Guessan A, T.A., Sanchez-Quete F, Goitom E, Reiling SJ, Galvez JH, Nguyen TL, Nguyen HTL,
620 Visentin F, Hachad M, Krylova K, Matthews S, Kraemer SA, Stretenowich P, Bourgey M,
621 Djambazian H, Chen S, Roy A, Brookes B, Lee S, Simon M, Maere T, Vanrolleghem PA, Labelle M,
622 Moreira S, Levade I, Bourque G, Ragoussis J, Dorner S, Frigon D, Shapiro BJ. Detection of
623 prevalent SARS-CoV-2 variant lineages in wastewater and clinical sequences from cities in
624 Québec, Canada. *medRxiv* (2022).
- 625 53. Gerstung, M. *et al.* Reliable detection of subclonal single-nucleotide variants in tumour cell
626 populations. *Nat Commun* **3**, 811 (2012).
- 627 54. Rao, R.S.P. *et al.* Evolutionary Dynamics of Indels in SARS-CoV-2 Spike Glycoprotein. *Evol*
628 *Bioinform Online* **17**, 11769343211064616 (2021).
- 629 55. Ramachandran, V.K. *et al.* Comparison of variant callers for wastewater-based epidemiology.
630 *medRxiv* (2022).
- 631 56. Li, H. Aligning sequence reads, clone sequences and assembly contigs with BWA-MEM. *arXiv*
632 (2013).
- 633 57. McLaren, W. *et al.* The Ensembl Variant Effect Predictor. *Genome Biol* **17**, 122 (2016).
- 634